Geophys. J. Int. (1991) **104,** 135–146

3-D spatial variation of *b*-values of magnitude–frequency distribution beneath the Kanto District, Japan

Yosihiko Ogata,[1,2] Masajiro Imoto[2] and Koichi Katsura[1]

[1] *Institute of Statistical Mathematics, Minami-Azabu* 4-6-7, *Minato-ku, Tokyo* 106, *Japan*
[2] *National Research Center for Disaster Prevention, Tennodai* 3-1, *Tsukuba-city, Ibaraki-Prefecture* 305, *Japan*

Accepted 1990 July 31. Received 1990 July 25; in original form 1989 November 1

SUMMARY

A method is developed for estimation and interpolation of *b*-values in space. A 3-D spline function is considered for the logarithm of the *b*-value at each location in the space. Since many parameters for the spline coefficients are required to obtain a sensible estimate of the spatial variation of *b*-values, we consider the penalized log-likelihood with the standard roughness penalties for the spline function. Further the error bands of the *b*-value estimation at each location can be calculated. Using the current method, the spatial distribution of *b*-values beneath the Kanto District down to the depth of 100 km is determined based on hypocentral data of microearthquakes from the Kanto–Tokai Observational Network of the National Research Center for Disaster Prevention. The stability of the estimated pattern is checked by comparing with the results using alternative cut-off magnitudes. This is further ensured by comparison with the result obtained by an alternative model using equally divided blocks. On the whole, the vertical change in *b*-value is greater than the horizontal one. It is high in the crust of the Eurasian plate, especially above the upper boundary of the subducting Pacific plate and in the northwest part, or the volcanic area, in the Kanto District. A steep decrease of the *b*-values is seen to take place in perpendicular direction to the subducting Pacific plate boundary. Also, a similar change is seen in the boundary between the Eurasian and Phillippine Sea plates, especially beneath the southern part of the Kanto Plain. The *b*-value is low in the upper boundary of the subducting plates, but high in the lower plane of the double seismic zone in the Pacific plate. It appears that, even within a narrow area of aftershocks, the *b*-value can change significantly. It is also found that the variation of the *b*-value estimate is in good agreement with the structure of seismic wave fractional velocity perturbations. The regions of high and low *b*-values correspond, respectively, to the lower and higher parts of the *P*-wave velocity. The similar relationship is seen with the spatial structure of the seismic wave attenuation.

Key words: B-splines, *b*-value, magnitude frequency, objective Bayesian method, penalized log-likelihood, smoothing, spatial magnitude distribution.

1 INTRODUCTION

Gutenberg & Richter (1944) observed the empirical law of the number $N(M)$ of earthquakes having magnitude M or larger such that

$$\log_{10} N(M) = a - bM. \tag{1}$$

The coefficient $-b$ corresponds the slope of the plot of $\log_{10} N(M)$ against magnitude M. This is a power law connecting the frequency distribution function with the energy release, and thus estimation of b is related to the estimation of the power-law index. Gutenberg & Richter (1954) reported estimates of the *b*-values for various regions of the world. According to Utsu (1971) more than 250 papers include descriptions of *b*-values and related quantities for earthquakes occurring in some regions of the world: regional variation of *b*-values of shallow earthquakes, variation of *b*-values with depth, and variation of *b*-values with time. Utsu (1971) summarizes that *b*-values vary roughly in the range 0.3–2.0. Anderson, Hasegawa &

Takagi (1980) discuss 1-D variation of b-values with depth in the upper plane of the deep seismic zone along the subducting Pacific plate against the Eurasian plate beneath Tohoku District, Japan, using the data from the microearthquake network of Tohoku University.

The spatial distribution of earthquakes beneath the Kanto District seems more complicated than beneath Tohoku and has been interpreted by the occurrence owing to the interaction among the Philippine Sea (PHS), the Eurasian (EUR), and the Pacific (PAC) plates: see Fig 1(a–c) for the distribution of hypocentres beneath the Kanto Plain. A rough sketch of the interacting plates beneath the Kanto District for interpreting the tectonics of the areas is outlined as follows (see Fig. 1d): the PHS plate subducts under the EUR plate from the Sagami and Suruga troughs toward the northwest, the PAC plate subducts under the EUR and PHS plates from the Japan and Izu–Bonin trenches toward the west–northwest. The eastern edge of the PHS plate is laid on the PAC plate and generates high seismicity in SW Ibaraki and Middle Chiba Prefectures (about the centre along 140°E in Fig. 1a). The central part of the PHS plate is colliding against the EUR plate, the north of the Izu Peninsula. The hypocentre distribution of high resolution in Fig. 1(a–c) clearly shows some characteristic features of seismicity in the Kanto area: the double seismic planes associated with the subducting PAC plate, clusters of deep foci in SW Ibaraki and middle Chiba. The delineation of the plates' configuration has been discussed by Nakamura, Shimazaki & Yonekura (1984), Maki (1984), Noguchi (1985), Kasahara (1985) and Ishida (1986).

Although these models give the rough framework of the tectonics of the Kanto area, they still leave some ambiguities in fine detail, especially at the edges of the rubbing plates. In this paper we look at the spatial variation of b-values of these zones in the hope that this will give some useful information on such details. This has considerable potential because, as is seen later, the resolution of b-values is high at the regions of high seismicity in the zones of contacting slabs.

2 ESTIMATION METHOD

A large number of parameters is needed to represent the variation of b-values in time or space, whether they are the values at the divided sub-blocks (Imoto & Ishiguro 1986) or the coefficients of a spline function (Ogata & Katsura 1988) on the considered regions. For the parameter estimation, we maximize the log-likelihood function which measures the goodness of fit to the data. On the other hand, to get a stable and sensible estimate of such a large number of the parameters, constraint among the parameters has to be assumed. In the present paper, the constraint called the

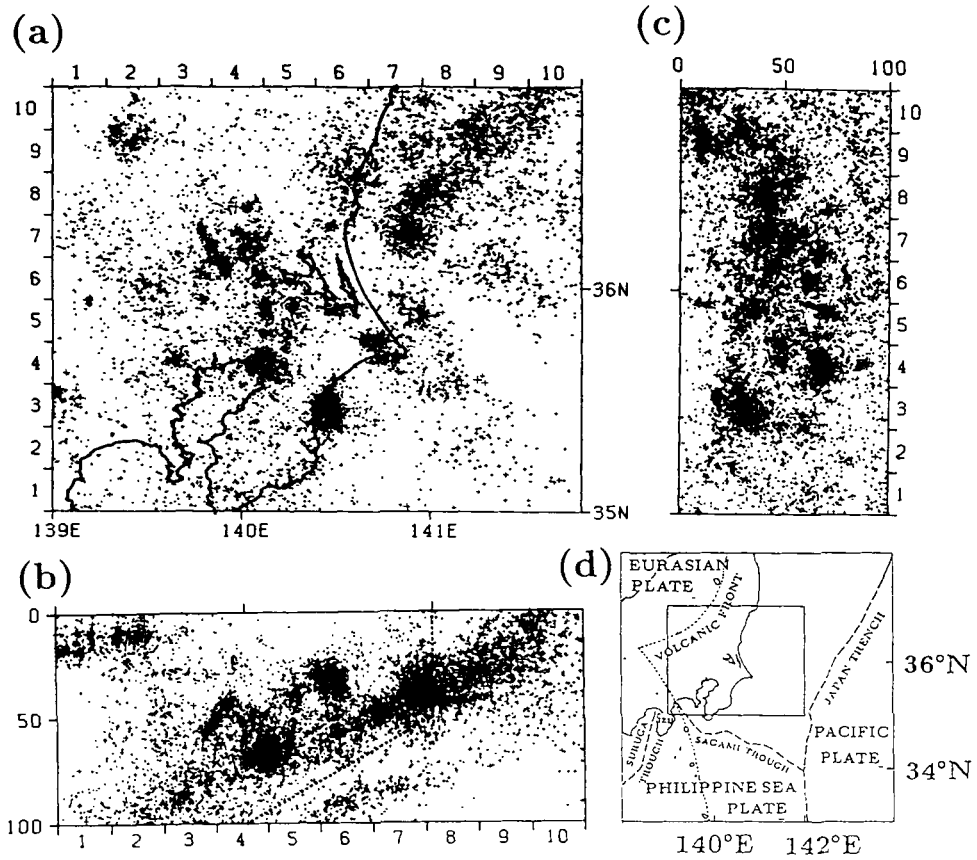

Figure 1. Hypocentral distributions of microearthquakes beneath Kanto Plain. (a) Projection to the horizontal plane. The numbers 1–10 on the left and top edges correspond to profile numbers of vertical sections in Figs 5–7. (b) Projection to the west–east vertical plane. (c) Projection to the north–south vertical plane. (d) Map of the Kanto District and its tectonic setting. The Sagami and Suruga troughs represent the boundary between the Eurasian and Philippine Sea plates in the Kanto District. The latter is a northern extension of the Nankai trough. The Philippine Sea plate is considered to subduct along those troughs and to collide with the Eurasian plate, north of the Izu Peninsula.

roughness penalty is measured by a sum of the integrated squares of first and second derivatives of the spline function. This is to be minimized to avoid unnecessary fluctuation of an estimated spline surface. Thus we have to resolve the trade-off between the two conflicting aims in surface estimation, which are to produce a good fit to the data but to avoid too much rapid fluctuation. For this purpose the idea of the so-called objective Bayesian method (Akaike 1980; Ishiguro & Sakamoto 1983) is very useful.

2.1 A model for spatial *b*-value estimation

For the efficient estimation of the b-value in (1), Utsu (1965) proposed the estimator $\hat{b} = I \log_{10} e / \sum_{i=1}^{I} (M_i - M_c)$, which was originally derived by the moment method, for the observation of magnitudes $\{M_i, i = 1, \ldots, I\}$, where M_c is the lowest bound of the magnitude above which almost all the earthquakes are detected. Aki (1965) showed that this estimator is the maximum likelihood estimate which maximizes the likelihood function

$$L(b) = \prod_{i=1}^{I} f(M_i \mid \beta), \tag{2}$$

where f is the exponential distribution

$$f(M \mid \beta) = \beta e^{-\beta(M - M_c)}, \qquad M > M_c, \tag{3}$$

and $\beta = b \log_e 10$.

In the present paper, we assume that the coefficient of the exponential distribution (3) is dependent on the location of the space and is therefore a function of a hypocentre (x, y, h) in such a way that

$$\beta = \beta_\theta(x, y, h), \tag{4}$$

where $\boldsymbol{\theta}$ is a parameter vector characterizing the function. Then, having observed the magnitude data M_i for each hypocentre's coordinate (x_i, y_i, h_i) with $i = 1, 2, \ldots, I$, the current likelihood function of $\boldsymbol{\theta}$ can be writen as

$$L(\boldsymbol{\theta}) = \prod_{i=1}^{I} \beta_\theta(x_i, y_i, h_i) e^{-\beta_\theta(x_i, y_i, h_i)(M_i - M_c)}, \qquad M_i > M_c. \tag{5}$$

Since β, or b, is positive valued, the parametrization of the function $\beta_\theta(x, y, h)$ is carried out by

$$\beta_\theta(x, y, h) = e^{\phi_\theta(x, y, h)} / \log_{10} e, \tag{6}$$

so that the estimate of b-values in space is given by

$$b_\theta(x, y, h) = e^{\phi_\theta(x, y, h)}, \tag{7}$$

where the ϕ is the 3-D B-spline function

$$\phi_\theta(x, y, h) = \sum_{l=0}^{L+3} \sum_{m=0}^{M+3} \sum_{n=0}^{N+3} c_{l,m,n} F_l(x) G_m(y) H_n(h). \tag{8}$$

The parameter $\boldsymbol{\theta} = \{c_{l,m,n}\}$ is a set of coefficients, and the functions F_l, G_m and H_n are cubic B-spline bases with equally spaced knots: see Section 2.3 for a detailed description. In this paper, if necessary, the coefficients $\boldsymbol{\theta} = \{c_{l,m,n}\}$ are suitably ordered to treat $\boldsymbol{\theta}$ as a vector, i.e., $\boldsymbol{\theta} = \{c_p\}$ such that $p = l(M + 3)(N + 3) + m(N + 3) + n$.

The smooth spline function is extremely useful for both fitting the irregularly sampled data on a space and for interpolating where no data is available. Further, since the spline is defined on local bases, this is computationally efficient compared to the globally defined hierarchical bases such as the ordinally (multivariate) polynomials.

2.2 The objective Bayesian method

Since a large number of parameters in the vector $\boldsymbol{\theta}$ are required for representing the 3-D spline function, the maximum likelihood estimate usually produces a rapidly fluctuated surface. Thus we had to resolve two conflicting aims in surface estimation, which are to produce a good fit to the data but to avoid too much rapid local variation. A measure of the local variation of a surface can be given by roughness penalties, or smoothness constraints, of the function $\phi = \phi_\theta(x, y, h)$ such that

$$\Phi_1(\boldsymbol{\theta} \mid w_1, w_3) = \int_V w_1 \left[\left(\frac{\partial \phi}{\partial x} \right)^2 + \left(\frac{\partial \phi}{\partial y} \right)^2 \right] + w_3 \left(\frac{\partial \phi}{\partial h} \right)^2 dx\, dy\, dh \tag{9}$$

and

$$\Phi_2(\boldsymbol{\theta} \mid w_2, w_4, w_5) = \int_V w_2 \left[\left(\frac{\partial^2 \phi}{\partial x^2} \right)^2 + 2 \left(\frac{\partial^2 \phi}{\partial x\, \partial y} \right)^2 + \left(\frac{\partial^2 \phi}{\partial y^2} \right)^2 \right] + w_4 \left[2 \left(\frac{\partial^2 \phi}{\partial x\, \partial h} \right)^2 + 2 \left(\frac{\partial^2 \phi}{\partial y\, \partial h} \right)^2 \right] + w_5 \left(\frac{\partial^2 \phi}{\partial h^2} \right)^2 dx\, dy\, dh, \tag{10}$$

where the non-negative constants $w_1, \ldots, w_5$ are weights controlling the strength of the penalties. These are extensions by Meinguet (1979) and Inoue (1986). Note here that, if $w_1 = w_3$ and $w_2 = w_4 = w_5$, the penalties are imposed isotropically. Here, we consider the possibility of non-isotropy such that isotropy in (x, y) plane still holds but not in the direction of depth h. Thus, for the suitable weights $w_1, \ldots, w_5$, the estimates of the parameters $\boldsymbol{\theta} = (c_{ijk})$ are obtained so as to maximize the penalized log-likelihood (Good & Gaskins 1971):

$$Q(\boldsymbol{\theta} \mid w_1, w_2, \ldots, w_5) = \log L(\boldsymbol{\theta}) - \Phi_1(\boldsymbol{\theta} \mid w_1, w_3) - \Phi_2(\boldsymbol{\theta} \mid w_2, w_4, w_5), \tag{11}$$

where, substituting (6) into (5) and then taking the logarithm of the both hand sides of the equation (5),

$$\log L(\boldsymbol{\theta}) = \sum_{i=1}^{I} [\phi_\theta(x_i, y_i, h_i) - e^{\phi_\theta(x_i, y_i, h_i)} (M_i - M_c) / \log_{10} e] - I \log_{10} e, \tag{12}$$

for the data set $\{(x_i, y_i, h_i, M_i); i = 1, 2, \ldots, I\}$. Incidentally, if the likelihood is a Gaussian regression, the negative log-likelihood is the *sum of squares*, and the standard ill-posed linear problems are usually reduced to the minimization of the quantity $-Q$, the so-called damped least squares (see Inoue *et al.* 1990, for example). But this is not really the case here because (5) is based on a non-Gaussian distribution, i.e. the exponential distribution.

If we take w_1 and w_3 being large enough, the estimated function is nearly a flat surface so as to avoid any trends. On the other hand, if we take w_2, w_4 and w_5 to be large enough,

the estimated function may have a global trend but with reduced undulation. In this way, the penalties are used as a measure to be minimized for avoiding unnecessary fluctuation of a spline surface. The determination of weights $w_1, w_2, \ldots, w_5$ for penalties in (9) and (10) is therefore crucial to our method.

To obtain the optimal weights, we are led to a Bayesian interpretation (Akaike 1980). That is to say, the exponential of the negative sum $-(\Phi_1 + \Phi_2)$ in (11) is considered to be proportional to the prior distribution $\pi(\boldsymbol{\theta} \mid w_1, w_2, \ldots, w_5)$ characterized by the hyperparameters $w_1, w_2, \ldots, w_5$. The penalties Φ_1 and Φ_2 are quadratic with respect to the parameters $\boldsymbol{\theta} = \{c_{ijk}\} = (c_p)_{p=1,2,\ldots,P}$ for some non-negative definite matrix $\Sigma = \Sigma(w_1, \ldots, w_5)$ such that

$$\tfrac{1}{2}\boldsymbol{\theta}\Sigma\boldsymbol{\theta}^{\mathrm{T}} = \Phi_1(\boldsymbol{\theta} \mid w_1, w_3) + \Phi_2(\boldsymbol{\theta} \mid w_2, w_4, w_5). \tag{13}$$

Therefore the prior π is a multivariate Gaussian distribution. However, it turns out that the matrix Σ degenerate and $\mathrm{rank}(\Sigma) = P - 1$ in the present case, which leads π to the improper prior with respect to $\boldsymbol{\theta}$. To avoid such difficulty, the parameter vector $\boldsymbol{\theta} = (c_p)_{p=1,2,\ldots,P}$ is divided into $(\mathbf{c}^r, c_P)$ so that $\pi(\mathbf{c}^r, c_P \mid w_1, w_2, \ldots, w_5)$ is proper with respect to $\mathbf{c}^r$ such that

$$\pi(\mathbf{c}^r \mid w_1, w_2, \ldots, w_5, c_P) = \frac{(\det \Sigma_r)^{1/2}}{\sqrt{2\pi}^{P-1}} \mathrm{e}^{-\boldsymbol{\theta}\Sigma\boldsymbol{\theta}^{\mathrm{T}}/2}, \tag{14}$$

where c_P is the last (scalar) component of $\boldsymbol{\theta}$, $\mathbf{c}^r$ is the rest, and Σ_r is the cofactor of the last diagonal element of Σ.

We then consider the integral of the posterior function with respect to $\mathbf{c}^r$,

$$\mathbf{L}(w_1, w_2, \ldots, w_5, c_P) = \int L(\theta)\pi(\mathbf{c}^r, c_P \mid w_1, w_2, \ldots, w_5)\, d\mathbf{c}^r, \tag{15}$$

to obtain $w_1, w_2, \ldots, w_5$ and c_P which maximize $\mathbf{L}$. This is called the method of *type II maximum likelihood* suggested by Good (1965). Akaike (1980) calls $\mathbf{L}$ in (15) *Bayesian likelihood*, justified and implemented the method based on the *entropy maximization principle* (Akaike 1977) and defined the *Akaike's Bayesian Information Criterion* as

$$ABIC = (-2) \max_{w_1,\ldots,w_5,c_P} \log \mathbf{L} + 2(\text{number of hyperparameters}), \tag{16}$$

in relation to the Akaike's Information Criterion (AIC; Akaike 1974). Here the number of hyperparameters in the present case is six which stands for $w_1, w_2, \ldots, w_5$ and c_P. A Bayesian model with a smaller *ABIC* value provides a better fit to the data.

Since the likelihood in (5) and its logarithm (12) are certainly based on non-Gaussian distribution, we cannot obtain analytic solution of the integral in (15) unlike the examples in Akaike (1980). Nevertheless, since the prior π is Gaussian, we may use the Gaussian approximation method suggested by Ishiguro & Sakamoto (1983). That is to say, the logarithm of the integrand in (15)

$$\begin{aligned} T(\boldsymbol{\theta}; w_1, w_2, \ldots, w_5) &= \log[L(\boldsymbol{\theta})\pi(\boldsymbol{\theta} \mid w_1, w_2, \ldots, w_5)], \\ &= Q(\boldsymbol{\theta} \mid w_1, w, \ldots, w_5) + \tfrac{1}{2}\log\det\Sigma_r \\ &\quad - \frac{P-1}{2}\log 2\pi \end{aligned} \tag{17}$$

is approximated by the quadratic form

$$\begin{aligned} T(\boldsymbol{\theta} \mid w_1, \ldots, w_5) \cong\ & T(\hat{\boldsymbol{\theta}} \mid w_1, \ldots, w_5) \\ & - \tfrac{1}{2}(\boldsymbol{\theta} - \hat{\boldsymbol{\theta}})\mathcal{H}(\hat{\boldsymbol{\theta}} \mid w_1, \ldots, w_5)(\boldsymbol{\theta} - \hat{\boldsymbol{\theta}})^{\mathrm{T}}, \end{aligned} \tag{18}$$

where $\hat{\boldsymbol{\theta}}$ is the vector which maximizes T, or Q, in (17) for fixed $w_1, w_2, \ldots, w_5$, and $\mathcal{H}(\hat{\boldsymbol{\theta}}; w_1, \ldots, w_5)$ is the Hessian matrix (i.e. second derivatives) of the penalized log-likelihood at $\hat{\boldsymbol{\theta}}$: that is,

$$\mathcal{H}(\hat{\boldsymbol{\theta}} \mid w_1, \ldots, w_5) = \frac{\partial^2 \log L(\hat{\boldsymbol{\theta}})}{\partial\boldsymbol{\theta}\,\partial\boldsymbol{\theta}^{\mathrm{T}}} - \tfrac{1}{2}\Sigma(w_1, \ldots, w_5) \tag{19}$$

from (11) and (13). Using the quadratic approximation in (18) and the equation in (19), we have an approximated log Bayesian likelihood given by

$$\begin{aligned} &\log \mathbf{L}(w_1, \ldots, w_5, \hat{c}_P) \\ &= T(\hat{\boldsymbol{\theta}} \mid w_1, \ldots, w_5) - \tfrac{1}{2}\log\{\det \mathcal{H}_r\} + \frac{P-1}{2}\log 2\pi \\ &= Q(\hat{\boldsymbol{\theta}} \mid w_1, \ldots, w_5) + \tfrac{1}{2}\log\{\det \Sigma_r\} - \tfrac{1}{2}\log\{\det \mathcal{H}_r\}, \end{aligned} \tag{20}$$

where P is the dimension of the parameter $\boldsymbol{\theta} = (\mathbf{c}^r, c_P)$, and $\mathcal{H}_r = \mathcal{H}_r(\mathbf{c}^r \mid w_1, \ldots, w_5)$ is the cofactor of the last diagonal element of $\mathcal{H}(\boldsymbol{\theta} \mid w_1, \ldots, w_5)$. It should be noted that the both maximization of log $\mathbf{L}$ in (20) and the penalized log-likelihood Q in (11) are non-linear. We use Davidon–Fletcher–Powell method (e.g., Fletcher & Powell 1963; Akaike *et al.* 1984) for maximizing Q in (11) with respect to the vector $\boldsymbol{\theta}$ of parameters for fixed $w_1, w_2, \ldots, w_5$. We also use the same optimization method, but using numerically calculated gradients, for maximizing (20) with respect to $w_1, w_2, \ldots, w_5$. This is repeated until the latter optimization converges. In maximizing Q in (11) with respect to $\boldsymbol{\theta}$ we found that the use of the Hessian $\mathcal{H}(\hat{\boldsymbol{\theta}} \mid w_1, w_2, \ldots, w_5)$ for the standard Newton–Raphson procedure in suitable stages (say, in the fifth or the tenth step) makes the convergence very rapid in spite of the large dimension of $\boldsymbol{\theta}$. This supports that the approximation (18) for (17) is good enough.

It is useful to get the estimation error of $b_{\hat{\theta}}(x, y, h)$ in (7) at any location (x, y, h). We know that joint error distribution of the parameters at $\hat{\boldsymbol{\theta}} = (\hat{c}_p)$ is approximately given by the multivariate normal $N(0, \mathcal{H}^{-1})$, where $\mathcal{H}^{-1} = (h^{p,p'})$ is the inverse of the same Hessian matrix $\mathcal{H} = (h_{p,p'})$ as in (18). Since $\phi_\theta(x, y, h)$ in (8) is given by the linear combination with respect to c_p, its error distribution is also expected to be approximately normal and the variance–covariance matrix between (x, y, h) and (x', y', h') is given by

$$C(x, y, h; x', y', h') = \sum_p \sum_{p'} h^{p,p'} F_l(x) G_m(y) H_n(h) F_{l'}(x') G_{m'}(y') H_{n'}(h'), \tag{21}$$

where $p = l(M+3)(N+3) + m(N+3) + n$ and $p' = l'(M+3)(N+3) + m'(N+3) + n'$ for $l, l' = 1, 2, \ldots, L+3$; $m, m' = 1, 2, \ldots, M+3$ and $n, n' = 1, 2, \ldots, N+3$. Thus

the standard error of $\phi_{\hat{\theta}}$ at (x, y, h) is

$$\varepsilon(x, y, h) = C(x, y, h; x, y, h)^{1/2}, \quad (22)$$

and the errors of $b_{\hat{\theta}}$ are given by the corresponding log normal distribution owing to relation (7). In a later section, to indicate the standard errors of the log normal distribution, we draw contours of the quantity

$$e_{\hat{\theta}} = \tfrac{1}{2}\{\exp[\phi_{\hat{\theta}}(x, y, h) + \varepsilon(x, y, h)] - \exp[\phi_{\hat{\theta}}(x, y, h) - \varepsilon(x, y, h)]\}. \quad (23)$$

2.3 Some remarks on the B-spline function

The 3-D spline function is constructed as follows. Consider the parallelopipedon $V = (x_0, x_L) \times (y_0, y_M) \times (h_0, h_N)$ for the domain of definition of the function; the sequences of points $x_0 < x_1 < \cdots < x_{L-1} < x_L$, $y_0 < y_1 < \cdots < y_{M-1} < y_M$ and $h_0 < h_1 < \cdots < h_{N-1} < h_N$ are equally spaced, respectively. All the segments (x_0, x_L), (y_0, y_M) and (h_0, h_N) are extended to (x_{-3}, x_{L+3}), (y_{-3}, y_{M+3}) and (h_{-3}, h_{N+3}), where $\{x_l; l = -3, -2, \ldots, L+3\}$, $\{y_m; m = -3, -2, \ldots, M+3\}$ and $\{h_n; n = -3, -2, \ldots, N+3\}$ are again equally spaced by distances of $d_x = (x_L - x_0)/L$, $d_y = (y_M - y_0)/M$ and $d_h = (h_N - h_0)/N$, respectively. Consider the cubic B-spline bases $\{B_i(r); i = 1, 2, 3, 4\}$ on $[0, 1]$ such that

$$B_1(r) = r^3/6,$$
$$B_2(r) = (-3r^3 + 3r^2 + 3r + 1)/6,$$
$$B_3(r) = (3r^3 - 6r^2 + 4)/6,$$
$$B_4(r) = (-r^3 + 3r^3 - 3r + 1)/6. \quad (24)$$

Thus, for (x, y, h) in a subdivided parallelopiped blocks $(x_l, x_{l+1}) \times (y_m, y_{m+1}) \times (h_n, h_{n+1})$, the spline function is given by

$$\phi(x, y, h \mid \boldsymbol{\theta}) = \sum_{i=0}^{3}\sum_{j=0}^{3}\sum_{k=0}^{3} c_{l+i,m+j,n+k} B_{4-i}(r_x) B_{4-j}(r_y) B_{4-k}(r_h), \quad (25)$$

where $\boldsymbol{\theta} = \{c_{ijk}\}$ are coefficients, $r_x = (x - x_l)/d_x$, $r_y = (y - y_m)/d_y$ and $r_h = (h - h_n)/d_h$.

One of the advantages of this spline is that the roughness penalties $\Phi_1(h)$ and $\Phi_2(h)$ in (3.1) and (3.2) reduce to the integrals $\int_0^1 B_i' B_j' \, dr$ and $\int_0^1 B_i'' B_j'' \, dr$, where the dashes indicate the derivatives with respect to r [see Inoue (1986) for the details].

Finally it is found that the standard error $\varepsilon(x, y, h)$ in (22) for the case where $h(x, y, h) = constant$ is slightly cyclic with spatial period $(d_x/2, d_y/2, d_h/2)$. This is due to the quadratic form of (21) with respect to the spline bases. To remove the cyclicity we use $[\varepsilon(x + d_x/4, y + d_y/4, h + d_h/4) + \varepsilon(x - d_x/4, y - d_y/4, h - d_h/4)]/2$ instead of $\varepsilon(x, y, h)$.

3 THE DATA

In this study we use the data of hypocentre coordinates and magnitudes of microearthquakes compiled by the National Research Center for Disaster Prevention (NRCDP) based on the Kanto–Tokai Network catalogue of the NRCDP. Detectability and accuracy of the source parameters of the microearthquakes by the network of NRCDP is discussed in Matsumura (1984) and Papanastassiou & Matsumura (1987). They conclude that the most earthquakes with a magnitude greater than 2.00 are detected beneath the Kanto Plain down to 100 km depth: the standard deviations are less than a few kilometres for the determination of epicentres and the focal depth.

Taking into account the detection capability of the network, all events above magnitude $M = 2.00$ in the period from July 1983 to December 1988, with depth shallower than 100 km are considered in a region bounded by the 139°E and 142°E meridians, and the 35°N and 37°N parallels, which includes most of Kanto District (see Fig. 1d). The number of events in the region is 13528. Most of the shocks occurred on the boundary between the EUR, PAC and PHS plates. Fig. 1(a–c) shows hypocentres of these events during the period considered.

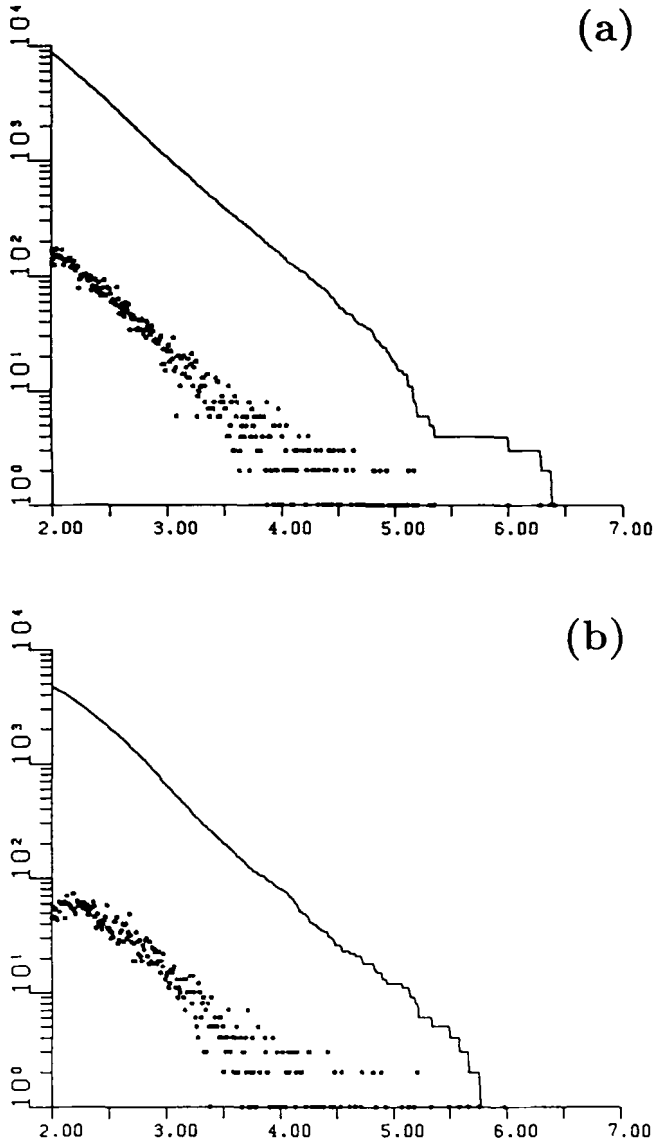

Figure 2. Magnitude–frequency distributions in (a) the western and (b) eastern subregion of the whole block divided by the planes in a parallel direction longitude, the projection of which is indicated by the dotted broken line in Fig. 1(b). The solid line shows the cumulative number, and dots indicate the numbers of earthquakes within the equally divided magnitude bands of length 0.01.

According to Matsumura (1984) and Papanastassiou & Matsumura (1987), the detectability is comparatively low beneath the offshore in Pacific area, due to being outside the network. Nevertheless, we include this area, since a large portion of the earthquakes take place along the subducting PAC plate. The whole 3-D region in Fig. 1(a–c) is divided into two parts by the two planes, being parallel to the N–S direction, the projection of which is indicated by the dotted line in Fig. 1(b). Fig. 2(a and b) shows the plots of magnitude versus logarithm of frequency of earthquakes in the considered time period and for the eastern and western parts of the whole block, respectively. The magnitude–frequency distribution in Fig. 2(a) shows that 2.0 is a suitable value for the cut-off magnitude M_c for the western part. For the eastern part, the frequency of microearthquakes in Fig. 2(b) attains the maximum at about $\hat{M} = 2.25$, and therefore $M_c = 2.5$ is taken for a suitable threshold. Thus we use two cut-off magnitudes depending on the aforementioned two blocks. That is, in the (log) likelihood (5) and (12), $M_c = 2.0$ for any i such that (x_i, y_i, h_i) belongs to the western part and $M_c = 2.5$ for the other i. Thus the number of considered events is reduced to 10870 in the whole block.

4 THE *b*-VALUE STRUCTURE

The area of Kanto District studied here (Fig. 1a) is the rectangle of about 250 km × 200 km in the directions of meridian and parallel, respectively, and from 0 km to 100 km in depth. This whole block is divided into $L \times M \times N = 10 \times 8 \times 4$ cubic sub-blocks with sides of 25 km length, for the knots of B-spline bases described in Section 2.3. Therefore the number of parameters $\boldsymbol{\theta} = \{c_{l,m,n}\}$ is $P = (L+3)(M+3)(N+3) = 1001$. At first the isotropical smoothness constraint within the whole block is assumed. This is interpreted by the penalty in (9) and (10) such that $w_1 = w_3$ and $w_2 = w_4 = w_5$, respectively. Thus the number of hyperparameters to maximize the Bayesian likelihood (15) is three. In this case $ABIC = 5485.4$ with $w_1 = 0.12$ and $w_2 = 0.26$. On the other hand, if we assume the non-isotropic roughness penalties in the direction of the depth against the horizontal planes, we need six independent hyperparameters to maximize the Bayesian likelihood, and we have $ABIC = 5432.8$ with $w_1 = 0.36$, $w_2 = 0.12 \times 10^{-2}$, $w_3 = 0.38 \times 10^{-2}$, $w_4 = 0.22 \times 10^{-3}$ and $w_5 = 0.17 \times 10^{-4}$. The significant improvement of the $ABIC$ suggests that the latter assumption is the better one to be adopted in the present case, and this indicates that the variation of b-values with depth is verly likely to be stronger than that in the horizontal sections. After all, we get the estimation of coefficients $\hat{\boldsymbol{\theta}} = (\hat{c}_{ijk})$ in (8), or explicitly in (25), by the maximization of (11). Thus we have made the profiles of the b-values beneath the Kanto District using relation (7).

To see the significance of the patterns of the b-values, the error distribution of the estimate is computed, and Fig. 3(a–c) shows the contours of the error bands for the middle cross-sections in respective directions of depth, east to west and south to north. The error distribution for b here is the log-normal (see the last paragraph in Section 2.2), and thus the contours drawn here are based on the quantity given in (23) with the modification described at the end of Section 2.3. In general the standard error is less than 0.1 in b-value around the highly clustered areas, and less than 0.2 in most areas except around the boundary of the region considered. Therefore the variation of b-values in the forthcoming figures is drawn by contours at intervals of 0.2.

Figure 4 includes the b-value distribution in the plane of horizontal cross-sections at depths 8, 16, 32, 48, 64, 80, 88 and 96 km, respectively. Fig. 5(a and b) shows profiles of the b-values in the plane of the vertical cross-sections of two directions, the parallel and meridian, respectively. The

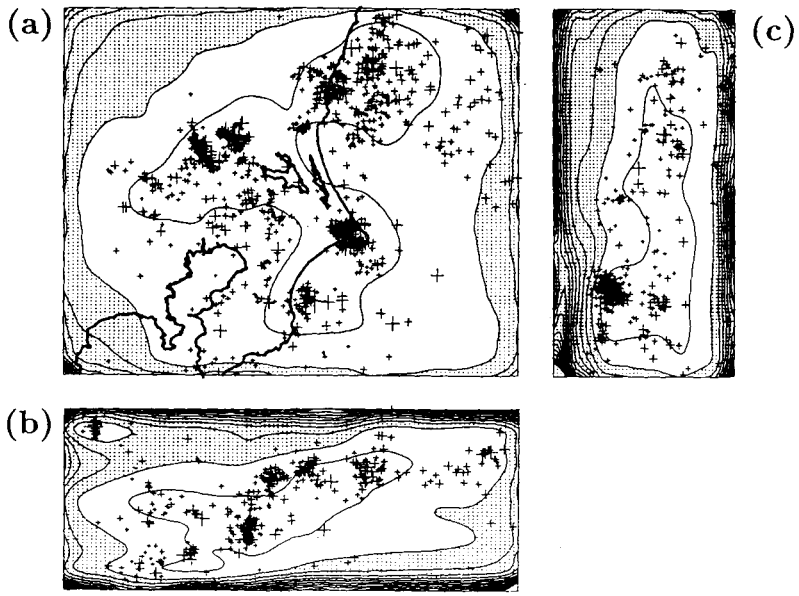

Figure 3. Standard error contours of the b-value estimate for each of (a) horizontal, (b) W–E vertical and (c) S–N vertical middle cross-sections. The contour interval is 0.1 and the shaded area shows the region where the standard error is greater than 0.2. Plotted hypocentres are within 4 km from each cross-section.

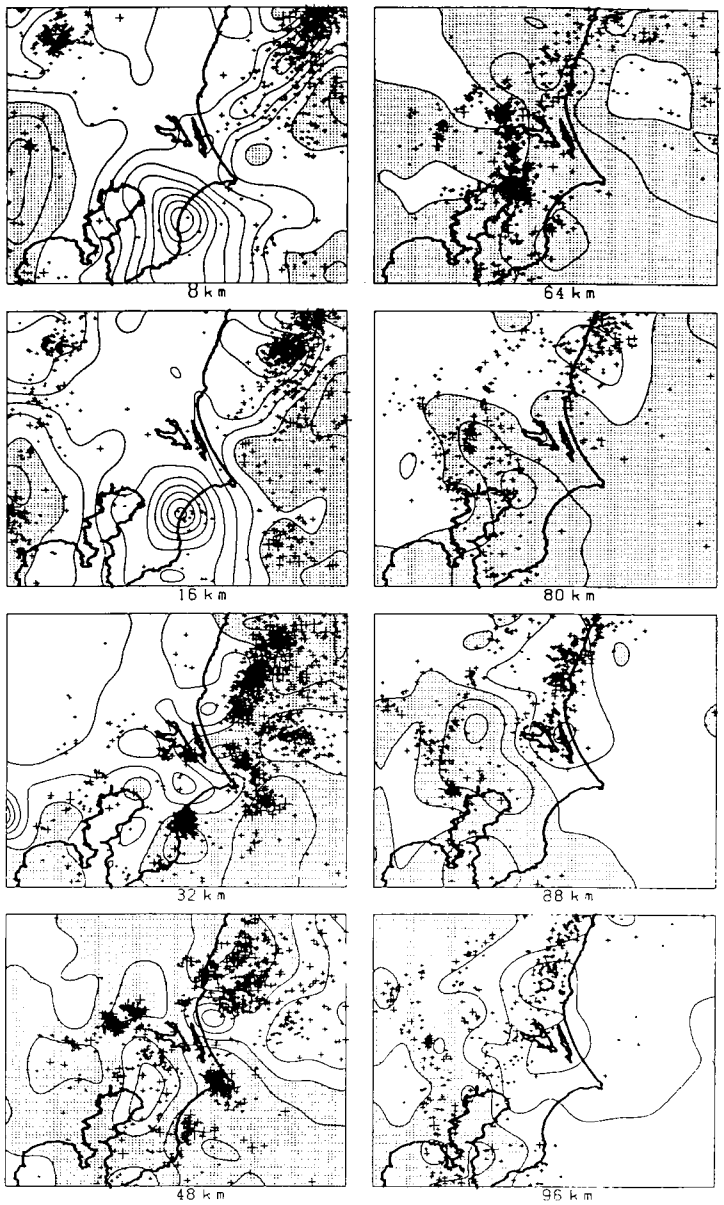

Figure 4. b-value contours in horizontal cross-sections at the depths 8, 16, 32, 48, 64, 80, 88 and 96 km. The contour interval is 0.2 and the shaded areas show regions where b is less than 1.0. Plotted epicentres are within 4 km in depth from each horizontal cross-section.

profile of hypocentres of the nearby earthquakes in each section is also shown. The attached numbers 1–10 at the left and top edges in Fig. 1(a) correspond to the profile numbers of the vertical sections in Fig. 5(a) and (b), respectively. The contour interval is 0.2 in b-value. The shaded areas show lower values than $b = 1.0$. In the following we describe the major characteristic of the b-value distribution.

On the whole, the vertical change in b-value is greater than the horizontal one. It is interesting and useful to see the estimated b-values in conjunction with the tectonic structure beneath the Kanto plain described in the Introduction. An apparent rapid reduction in b-values is found to take place in a direction perpendicular to the upper plane of subducting Pacific (PAC) plate (see Fig. 5, a1–5), especially beneath the southern half of the Kanto Plain, where the edge of the PHS plate is believed to overly the PAC plate. This boundary zone includes a number of aftershock areas of recent earthquakes with $M \geq 6.0$, that is, earthquakes of 1988 Eastern Tokyo, 1987 Off Chiba Prefecture, 1983 Ibaraki and 1980 Central Chiba Prefecture (see Table 1 for their characteristic parameters). In particular, the b-value changes within the aftershock area of the 1987 Off Chiba Prefecture earthquake is remarkable: it decreases rapidly with depth and increases towards the north (see Fig. 5, a3 and b6, and 32 km depth in Fig. 4). On the other hand, the b-value does not change much in the aftershock regions of the other interplate earthquakes.

It seems that b-values are low in the upper boundary of the subducting PAC plate beneath the northern half of the Kanto District where the PAC plate rubs against the crust of the Eurasian (EUR) plate: see the upper right part of Fig. 5 (a8–10 and b8–10). There, as depth increases, the b-values decrease in the upper seismic zone of PAC plate, but then the b-values become significantly higher in the lower part of

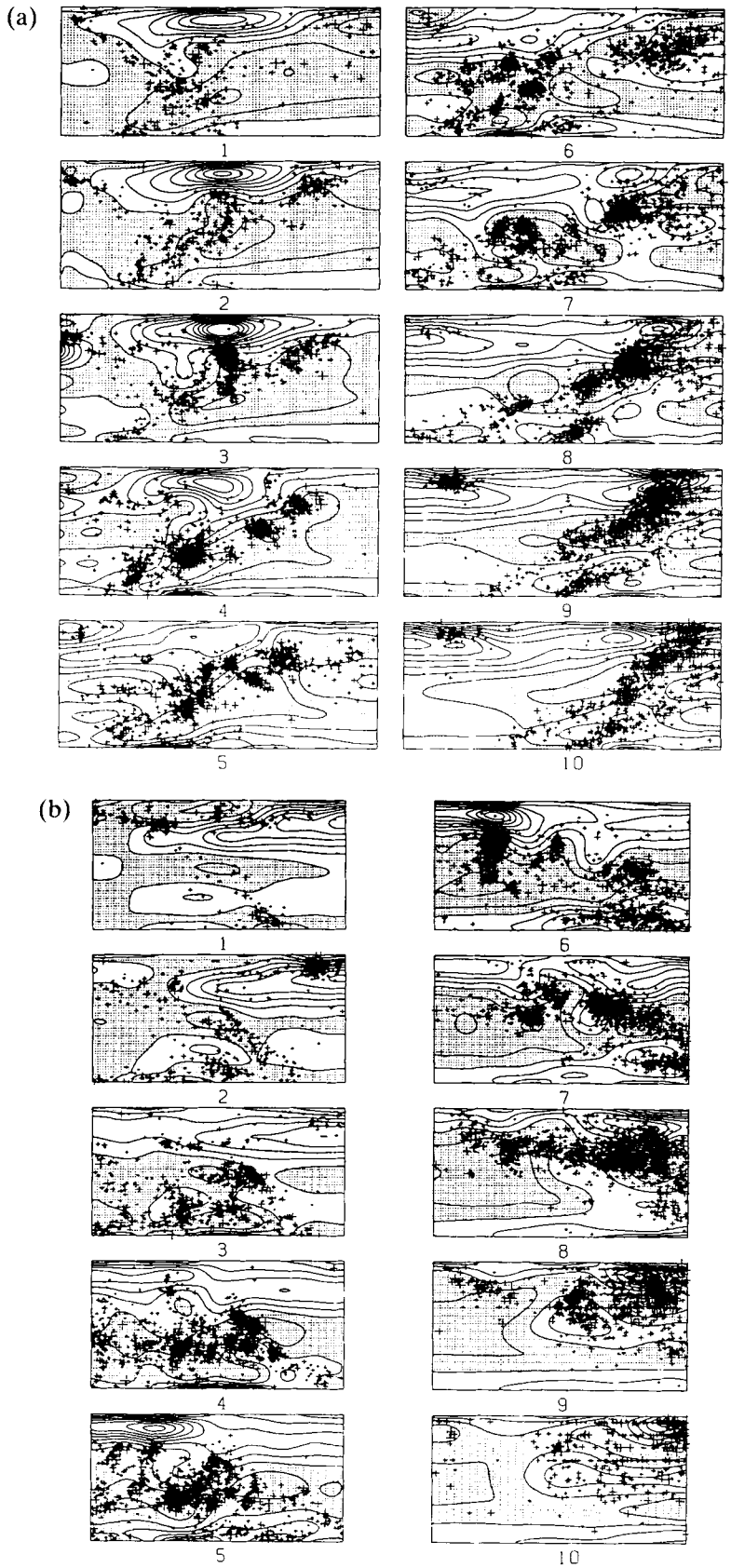

Figure 5. *b*-value contours in vertical cross-sections. 10 vertical cross-sections are made in parallel directions to (a) W–E and (b) S–N, respectively: each plane of cross-sections is in the middle of the 10 equally sliced volumes. The numbers below the figures are in order from south to north in the case of (a), and from west to east in the case of (b): see numbers 1–10 on the left and top edges of Fig. 1(a). The contour interval is 0.2 and the shaded area shows the region where *b* is less than 1.0. Plotted epicentres are within a sliced volume.

Table 1. Parameters of recent large earthquakes in the Kanto District.

Earthquakes	YR	MO	DY	M	LONG	LAT	DEP	Plates	Authors
E. Tokyo	88	03	18	6.4	139.63	35.67	90.5	PHS/PAC	Kasahara (1988)
E. Off Chiba Pref.	87	12	17	6.4	140.52	35.37	47.3	PHS/PAC	Okada (1988)
S. Ibaraki	85	10	04	6.1	140.11	35.91	71.6	PAC	Hori (1986)
E. Yamanashi Pref.	83	08	08	6.0	139.05	35.54	18.1	EUR/PHS?	
Ibaraki	83	02	27	6.0	140.10	35.97	69.	PHS/PAC	Ohtake & Kasahara(1983)
E. Off Ibaraki	82	07	23	7.0	142.20	36.36	8.5	EUR/PAC	Ohtake & Kasahara(1983)
C. Chiba Pref.	80	09	25	6.1	140.22	35.52	80.	PHS/PAC?	

the double seismic planes associated with subducting PAC plate at the depths of approximately 50–100 km (see the changes about the northern coast line at 80–100 km depth in Fig. 4 and at the lower parts of Fig. 5, a5–10 and b5–10).

The *b*-value of intraplate earthquakes in EUR is high: see 8, 16 and 32 km in Fig. 4, and the upper parts of Fig. 5(a). The volcanic area [see the volcanic front in Fig. 1(d)] in the northwest corner of the Kanto District has high *b*-values on the whole, but the values seem to rapidly increase as depth increases: see the top left of Fig. 5, a8–10 and the top right of Fig. 5, b1–3.

Along the subducting PHS plates beneath the EUR plate, the contour lines of *b*-values appear to be almost the same but low compared with those in EUR plate (see Fig. 5, a1–3 and b1–2). Here, a cluster of aftershocks of the Eastern Yamanashi Prefecture Earthquake is included (see the cluster at the upper left edge of Fig. 5, a3). The *b*-values within the aftershock area seem to rapidly increase as depth increases.

Besides the above features, there are many detailed changes which we cannot explain, especially beneath the central part of the Kanto District, where the resolution of the estimation is expected to be high. We don't know whether this shows any aspects of the suspected complex contact among the EUR and two subducting plates (see in particular Fig. 5, a3–7 and b3–7).

5 DISCUSSION

5.1 Stability of the result

To check the stability of the analysis, we obtained another estimate of *b*-values for a larger cut-off magnitude of $M_0 = 2.75$ by the same method as in the previous section. The number of data using the above threshold is 3049 in the whole block. The anisotropic penalties in (9) and (10) are supported also for the present data set by comparing the *ABIC* with that of the isotropic penalties. Figs 6(a) and (b) are provided here for comparison with Figs 5(a) and (b), respectively. The corresponding patterns are remarkably similar to each other except that the patterns in Figs 6(a) and (b) are rather simple. The same comparison is made among the patterns of a few other threshold magnitudes, and this similarity is seen among them. This suggests not only that the stability of the estimated pattern of *b*-values is guaranteed, but also that the regionally dependent magnitude thresholds in the previous section did not affect the pattern for the present data set: that is, the *b*-pattern is almost independent of the threshold magnitude.

It is useful to compare the estimate with that by an alternative method for the restricted area where the tectonic structure is expected to be most complex. To do this we used the same statistical model for *b*-value changes in time and 2-D space as used in Imoto (1987), except that the time axis is replaced by the depth axis. The block beneath the central Kanto District is divided into $14 \times 14 \times 10$ cubes with sides of 10 km length. For each divided cube, a parameter of the *b*-value is attached and then estimated by the similar Bayesian procedure (15)–(20) except that multinomial distribution, instead of the exponential, is used for the likelihood function for the data of categorized magnitudes between 2.0 and 4.0. Then, the estimates at each of the $14 \times 14 \times 10$ blocks are smoothed by contouring. Fig. 7 includes several *b*-value patterns of E–W cross-sections in the restricted block. Compare these with the corresponding figures of the same number in Fig. 5(a). In spite of the different parametrization, we can see some similarity in low-frequency patterns of *b*-value variation.

Since *b*-value variation with depth is stronger than in the horizontal sections, we remember the naive result of 1-D variation of *b*-values with depth by Anderson *et al.* (1980), which are mentioned in the Introduction. It shows significantly high *b*-values from the surface to 40 km depth. They drop to <0.7 from 40 to 70 km depth, then increase to >1.0 from 70 to 100 km. On average, in the horizontal variation, this result agrees very well with ours.

Two criticisms of our analysis have been raised. One of them concerns the possibility of *b*-value distortion due to the calibration of magnitudes affected by the heterogeneous 3-D distribution of seismic attenuation. Since the seismic stations of NRCDP are very dense in the Kanto–Tokai area and fixed throughout the observation period considered, we believe that the calibration provides at worst uniformly biased magnitudes in the same local region so that the *b*-value pattern itself is not distorted. The independence of the *b*-patterns from the cut-off magnitudes shown above demonstrates our belief. Nevertheless, we have to wait to give a conclusive answer until magnitudes can be redetermined by a correct model for the 3-D attenuation structure beneath the Kanto District.

The other criticism concerns a possibility that biases in the locations of hypocentres may be dependent on the magnitudes of the earthquakes, and that the pattern of *b*-values estimation is seriously affected. If this is the case, it will be particularly true where the resolution is high, that is, where the hypocentres are highly clustered. However, we think that these problems are not so serious in the major part of the block considered, and further we believe that such a low-frequency pattern of the *b*-value variation in Figs 4–7 cannot be significantly affected by this possibility. This is demonstrated by the similarity between the *b* patterns in Figs 5(a) and 7: the latter was obtained through parameters defined on the divided cubic blocks, within which the *b*-value is constant. Nevertheless, as mentioned in the Introduction, since our final goal is to find useful information describing the complex plate boundary beneath

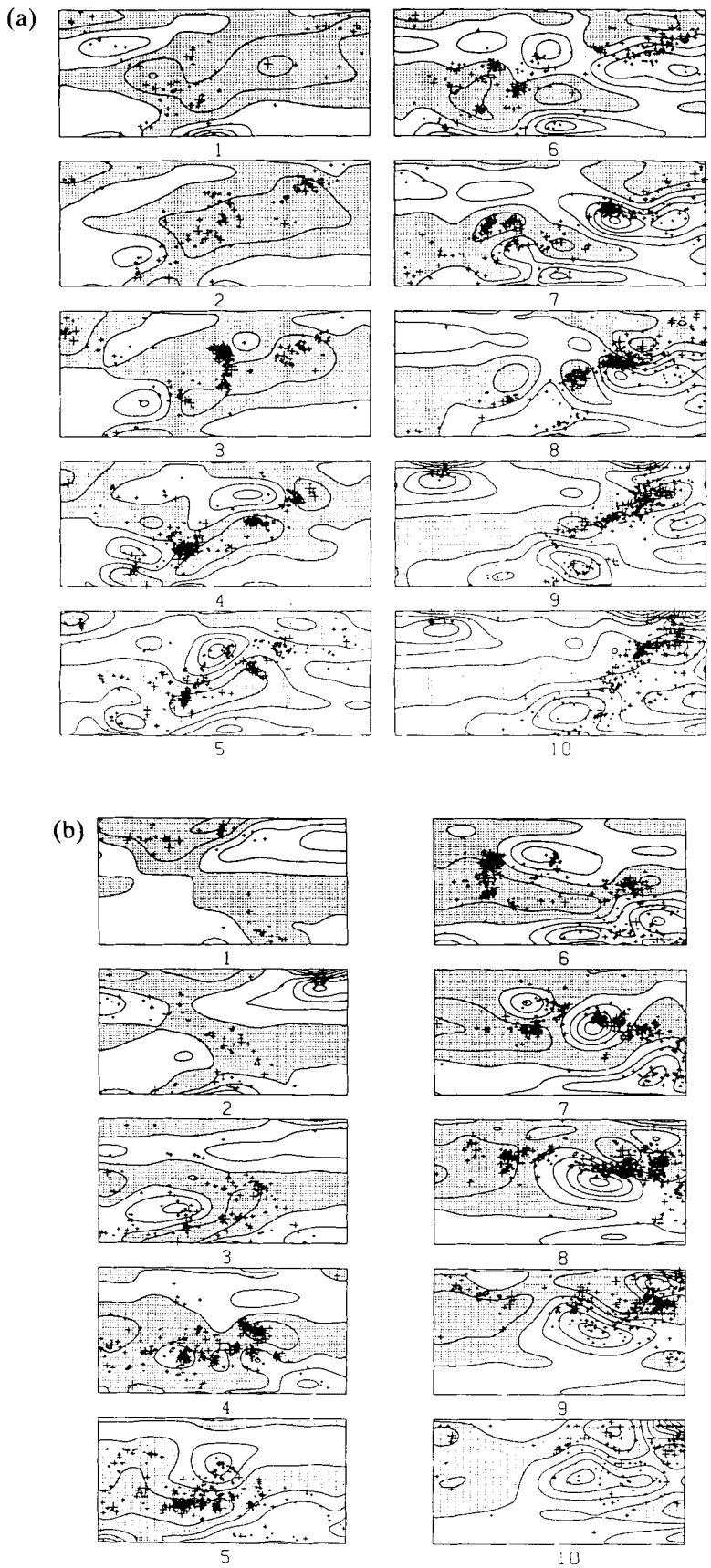

Figure 6. *b*-value contours in vertical cross-sections for the threshold magnitude $M_0 = 2.75$. (a) and (b) and the order of the figures are the same as in Fig. 5.

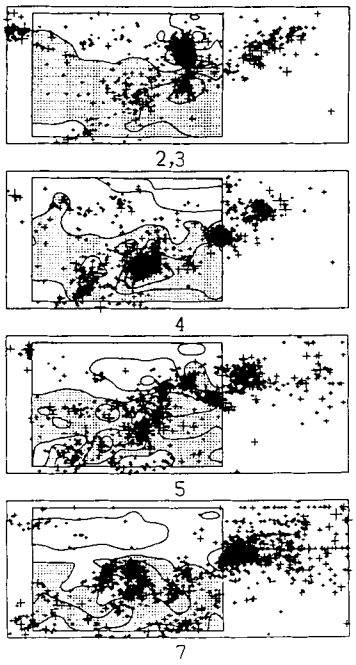

Figure 7. Contours of b-value in the W–E vertical sections obtained by the alternative method in the restricted area of central Kanto District. The number below each figure corresponds to that in Fig. 5(a). The contour interval is 0.2 and the shaded area shows the region of lower b-values than 1.0.

the Kanto District, this question is quite important, and therefore we are still investigating the effect of the b-value estimate due to the possible biases from relocated hypocentres. The results will be published elsewhere.

5.2 Comparison with other tomographical features

Comparing the whole pattern of interpolated b-value distribution with patterns of other geophysical quantities, it is found that the spatial variation of the b-value estimate is in remarkably good agreement with the structure of P-wave fractional velocity perturbations in the shallower part beneath the Kanto District: see figures of the corresponding profiles in Horie & Aki (1982) and Ishida & Hasemi (1988). Zones of high (low) b-values correspond to those of low (high) anomalies of the P-wave velocity, but the correlation in the deep part is not clear.

A similar relationship can be seen with the spatial structure of the seismic wave attenuation. Hashida & Shimazaki (1985) obtained a map of the deviation of the S-wave attenuation from the standard attenuation coefficient by inverting the intensity data. The high and low attenuation deviation is roughly in agreement with those of low and high b-values, respectively: compare the graphs of the corresponding profiles.

The agreement may not be so surprising, since the configuration of the plates can reflect the distribution of P- and S-wave velocity beneath the Kanto District, and also since we have seen that the b-value appears to change at the plate boundary.

6 CONCLUSIONS

An objective method is developed for estimation and interpolation of b-values at any location in space. A 3-D spline function is considered for the logarithm of b-value at each location in the space. Since many parameters for the spline coefficients are required to obtain sensible estimates of the b-value variation, we consider the penalized log-likelihood with the standard roughness penalties for the spline function. Weights for the penalties are adjusted objectively by maximizing the so-called Bayesian likelihood through a Bayesian interpretation of the penalized likelihood. The error bands of the b-value estimation at each location are calculated from the Hessian matrix of the optimal posterior distribution. The stability of the estimated pattern is successfully examined by comparing the estimate with that by higher threshold magnitudes and by an alternative parametrization for a central part of the Kanto District.

On the whole, the vertical change in b-value is greater than the horizontal one. It appears that, even within a narrow area of aftershocks, the b-value can change significantly. The b-value is low in the upper boundary of subducting PAC plates, but high in the lower part of the double seismic planes, which is within the plate. It is high in the crust of the EUR plate particularly in the upper part of the subducting PAC plate and in the northwest part, or a volcanic area, of the Kanto District. A steep decreasing change of the b-values is found to take place in the direction perpendicular to the subducting PAC plate. Also along the zone of the subducting PHS plates the b-value appears to be low, particularly beneath the southern part of the Kanto Plain. The rapidly changing b-values especially in the depth direction beneath the central part of the Kanto District seem to be a reflection of the suspected complex contact between the EUR and the two subducting plates. It is also found that the whole variation of b-values is in good agreement with the structure of P-wave fractional velocity perturbations in the shallower part of the region. The regions of high and low b-values correspond to those of lower and higher P-wave velocity, respectively, and also correspond to high and low anomalies of S-wave attenuation, respectively.

ACKNOWLEDGMENTS

This work was carried out while one of the authors (Y.O.) was a guest Research Associate at the National Research Center for Disaster Prevention as a member of the Project of the Science and Technology Agency of Japan entitled 'Earthquake fracture and wave propagation in heterogeneous structure of the earth' for 1988–1990. The authors are greatly indebted to Dr Haruo Sato, the leader of the project, for the encouragement of the present research. Also, Y. O. would like to thank Professor Tokuji Utsu for the useful information and helpful discussions on the present paper. Finally, the authors would like to thank the referee for helpful comments.

REFERENCES

Akaike, H., 1974. A new look at the statistical model identification, *IEEE Trans. Automat. Control*, AC – **19**, 716–723.

Akaike, H., 1977. On entropy maximization principle, in *Application of Statistics*, pp. 27–41, ed. Krishnaiah, P. R., North-Holland, Amsterdam.

Akaike, H., 1980. Likelihood and Bayes procedure, in *Bayesisn Statistics*, eds Bernard, J. M., De Groot, M. H., Lindley, D. U. & Smith, A. F. M., University Press, Valencia, Spain.

Akaike, H., Ozaki, T., Ishiguro, M., Ogata, Y., Kitagawa, G., Tamura, Y. H., Arahata, E., Katsura, K. & Tamura, Y., 1984. *Time Series and Control Program Package, TIMSAC-84*, Institute of Statistical Mathematics, Tokyo.

Aki, K., 1965. Maximum likelihood estimate of b in the formula $\log N = a - bM$ and its confidence limits, *Bull. Earthq. Res. Inst. Univ. Tokyo*, **43,** 237–239.

Anderson, R. N., Hasegawa, A. & Takagi, A., 1980. Phase changes and the frequency–magnitude distribution in the upper plane of the deep seismic zone beneath Tohoku, Japan, *J. geophys. Res.*, **83,** 1389–1398.

Fletcher, R. & Powell, M. J. D., 1963. A rapidly convergent descent method for minimization, *Comput. J.*, **6,** 163–168.

Good, I. J., 1965. *The Estimation of Probabilities*, MIT Press, Cambridge, MA.

Good, I. J. & Gaskins, R. A., 1971. Nonparametric roughness penalties for probability densities, *Biometrika*, **58,** 255–277.

Gutenberg, R. & Richter, C. F., 1944. Frequency of earthquakes in California, *Bull. seism. Soc. Am.*, **34,** 185–188.

Gutenberg, R. & Richter, C. F., 1954. *Seismicity of the Earth and Associated Phenomena*, 2nd edn, Princeton University Press, Princeton, NJ.

Hashida, T. & Shimazaki, K., 1985. Seismic tomography: 3D attenuation image of upper mantle structure beneath the Kanto District, Japan, *Earth planet. Sci. Lett.* **75,** 403–409.

Hori, S., 1986. The earthquake mechanism of the M 6.1 event occurred near the border of Chiba and Ibaraki Prefectures, central Japan, on October 4, 1985 and its tectonic implication, *Zisin II*, **39,** 457–468 (in Japanese).

Horie, A. & Aki, K., 1982. Three-dimensional velocity structure beneath the Kanto District, Japan, *J. Phys. Earth*, **30,** 255–281.

Imoto, M., 1987. Time–space variations of magnitudes–frequency relation in the Tokai area, *Zisin II*, **40,** 19–26 (in Japanese).

Imoto, M. & Ishiguro, M., 1986. A Bayesian approach to the detection of changes in the magnitude–frequency relation of earthquake, *J. Phys. Earth*, **34,** 441–455.

Inoue, H., 1986. A least squares smooth fitting for irregularly spaced data: Finite element approach using B-spline basis, *Geophysics*, **51,** 2051–2066.

Inoue, H., Fukao, Y., Tanabe, K. & Ogata, Y., 1990. Whole mantle P-wave travel time tomography, *Phys. Earth planet. Inter.* **59,** 294–328.

Ishida, M., 1986. The configuration of the Philippine Sea and the Pacific plates as estimated from the high-resolution microearthquake hypocenters in the Kanto–Tokai district, Japan, *Rep. NRCDP*, vol. 36, pp. 1–19, National Research Center for Disaster Prevention, Tsukuba, Japan (in Japanese).

Ishida, M. & Hasemi, A. H., 1988. Three-dimensional fine velocity structure and hypocentral distribution of earthquakes beneath the Kanto–Tokai district, Japan, *J. geophys. Res.*, **93,** 2076–2094.

Ishiguro, M. & Sakamoto, Y., 1983. A Bayesian approach to binary response curve estimation, *Ann. Inst. Statist. Math.*, **35,** 115–137.

Kasahara, K., 1985. Patterns of crustal activity associated with the convergence of three plates in the Kanto-Tokai area, central Japan, *Rep. NRCDP* 35, pp. 33–137, National Research Center for Disaster Prevention, Tsukuba, Japan (in Japanses).

Kasahara, K., 1988. The Eastern Tokyo Earthquake (M6.0) of March 18, 1988, *Report of the Coordinating Committee for Earthquake Prediction*, vol. 40, pp. 99–105, ed. Geographical Survey Institute, Ministry of Construction, Tsukuba, Japan.

Maki, T., 1984. Focal mechanisms and spatial distribution of intermediate-depth earthquakes beneath the Kanto District and vicinity with relation to the double seismic planes, *Bull. Earthq. Res. Inst. Univ. Tokyo*, **59,** 1–51.

Matsumura, S., 1984. Evaluation of detection capability of microearthquakes for an observational network: the Kanto–Tokai observational network of the National Research Center for Disaster Prevention, *Zisin II*, **37,** 475–489 (in Japanese).

Meinguet, J., 1979. Multivariate interpolation at arbitary points made simple, *Z. Angew. Math. Phys.*, **30,** 292–304.

Nakamura, K., Shimazaki, K. & Yonekura, N., 1984. Subduction bending and eduction; Present and Quaternary tectonics of the northern border of the Philippine Sea plate, *Bull. Soc. Geol. Fr.*, **26,** 224–243.

Noguchi, S., 1985. Configuration of Philippine Sea plate and seismic activities beneath Ibaraki Prefecture, *Earth Mon.*, **7,** 97–104 (in Japanses).

Ogata, Y. & Katsura, K., 1988. Likelihood analysis of spatial inhomogeneity for marked point patterns, *Ann. Inst. Math. Statist.*, **40,** 29–39.

Ohtake, M., 1986. Synchronized occurrence of offshore and inland earthquakes in the Ibaraki region, central Japan, *Earthq. Predict. Res.*, **4,** 165–174.

Ohtake, M. & Kasahara, K., 1983. Paired earthquakes in the Ibaraki Region, central Japan, *Zisin II*, **36,** 643–653 (in Japanese).

Okada, Y., 1988. Chibaken-Toho-Oki Earthquake of December 17, 1987, *Report of the Coordinating Committee for Earthquake Prediction*, vol. 40, pp. 81–86, ed. Geographical Survey Institute, Ministry of Construction, Tsukuba, Japan.

Papanastassiou, D. & Matsumura, S., 1987. Examination of the NRCDP's (The National Research Center for Disaster Prevention) seismic observational network as regards (1) detectability–locatability (2) accuracy of the determination of earthquake source parameters, *Report of the National Research Center for Disaster Prevention*, No. 39 pp. 37–65, Tsukuba, Japan.

Utsu, T., 1965. A method for determining the value of b in a formula $\log n = a - bM$ showing the magnitude frequency relation for earthquakes, *Geophys. Bull. Hokkaido Univ.*, **13,** 99–103 (in Japanese).

Utsu, T., 1971. Aftershock and earthquake statistic (III): Analyses of the distribution of earthquakes in magnitude, time and space with special consideration to clustering characteristics of earthquake occurrence (1), *J. Faculty Sci., Hokkaido University, Ser. VII (Geophys.)*, **3,** 379–441.